41. L. M. Cathles, *Econ. Geol.* **75th Anniv. Vol.**, 439 (1983), figure 6.
42. See M. Hovland and A. G. Judd in (*2*); J. M. Hunt, *Geochim. Cosmochim. Acta* **53**, 217 (1989).
43. J. M. Brooks, M. C. Kennicutt II, R. R. Fay, T. J. McDonald, R. Sassen, *Science* **225**, 409 (1984).
44. J. M. Brooks *et al.*, *Eos* **68**, 498 (1987); K. A. Kvenvolden, L. A. Barnard, J. M. Brooks, D. A. Wiesenberg, in *Advances in Organic Geochemistry, 1981*, M. Bjoroy *et al.*, Eds. (Wiley, New York, 1983), pp. 422–430.
45. K. A. Kvenvolden, *Chem. Geol.* **71**, 41 (1988).
46. As reported in *Eos* **66** (5 March 1985), p. 106.
47. C. W. Kreitler, *J. Hydrol.* **106**, 29 (1989).
48. P. A. Domenico and V. V. Palciauskas, in (*15*), pp. 435–445.
49. This view has been advanced particularly on the basis of the work of J. S. Bradley and D. E. Powley as reported recently by J. M. Hunt, *Am. Assoc. Pet. Geol. Bull.* **74**, 1 (1990).
50. G. Demaison, in *Petroleum Generation and Basin Evaluation*, G. Demaison and R. J. Murris, Eds. (American Association of Petroleum Geologists Memoir 35, Tulsa, 1984), pp. 1–14.
51. B. Durand, *Org. Geochem.* **13**, 445 (1988).
52. B. Tissot, in *Migration of Hydrocarbons in Sedimentary Basins*, B. Doligez, Ed. (Editions Technip, Paris, 1987), pp. 1–19.
53. S. H. Davis, S. Rosenblatt, J. R. Wood, T. A. Hewett, *Am. J. Sci.* **285**, 207 (1985).
54. L. S. Land, in *Clastic Diagenesis*, D. A. McDonald and R. C. Surdam, Eds. (American Association of Petroleum Geologists Memoir 37, Tulsa, 1984), p. 47.
55. P. Ungerer, E. Behar, D. Discamps, in *Advances in Organic Geochemistry, 1981*, M. Bjoroy *et al.*, Eds. (Wiley, New York, 1983), pp. 129–135.
56. H. D. Hedberg, in *Problems in Petroleum Migration*, W. H. Roberts and J. R. Cordell, Eds. (Studies in Geology No. 10, American Association of Petroleum Geologists, Tulsa, 1980), p. 179.
57. W. E. Galloway, *Econ. Geol.* **73**, 1655 (1978); M. B. Goldhaber, R. L. Reynolds, R. O. Rye, *ibid.*, p. 1690; W. E. Galloway, *Tex. Bur. Econ. Geol. Rep. Invest.* **119**, 1 (1982).
58. M. R. Ulrich *et al.*, *Trans. Gulf Coast Assoc. Geol. Soc.* **34**, 435 (1984).
59. Calculated from the seven small sulfide bands in 11 cm of anhydrite cap of the Hockley dome in Texas reported in (*60*), assuming the cap growth rate was similar to the ~5 m per 10^6 years paleomagnetically determined for the Winnfield dome in Louisiana [J. R. Kyle, M. R. Ulrich, W. A. Gose, in *Dynamical Geology of Salt and Related Structures*, I. Lerche and J. J. O'Brien, Eds. (Academic Press, New York, 1987), pp. 497–542].
60. W. S. Hallager, M. R. Ulrich, J. R. Kyle, P. E. Price, W. A. Gose, *Geology*, in press.
61. S. A. Jackson and F. W. Beales, *Bull. Can. Pet. Geol.* **15**, 383 (1967); J. M. Sharp, *Econ. Geol.* **73**, 1057 (1978); L. M. Cathles and A. T. Smith, *ibid.* **78**, 983 (1983); L. Cathles, *Appl. Geochem.* **2**, 649 (1987).
62. M. A. Etheridge, V. J. Wall, R. H. Vernon, *J. Metamorph. Geol.* **1**, 205 (1983); M. A. Etheridge, V. J. Wall, S. F. Cox, R. H. Vernon, *J. Geophys. Res.* **89**, 4344 (1984); S. F. Cox, M. A. Etheridge, V. J. Wall, *Ore Geol. Rev.* **2**, 65 (1986).
63. W. S. Fyfe and R. Kerrich, in *Gold '82: The Geology, Geochemistry and Genesis of Gold Deposits*, R. P. Foster, Ed. (Proceedings of the Gold '82 Symposium, University of Zimbabwe) (Geological Society of Zimbabwe, Rotterdam, 1983), pp. 99–127; L. M. Cathles, in *Gold in the Western Shield*, L. A. Clark, Ed. (special vol. 38, Canadian Institute of Mining and Metallurgy, Saskatoon, 1986), p. 187; R. Kerrich, *Geology* **17**, 1011 (1989).
64. R. C. Newton, J. V. Smith, B. V. Windley, *Nature* **288**, 45 (1980); R. C. Newton, *Annu. Rev. Earth Planet. Sci.* **17**, 385 (1989).
65. J. Oliver, *Geology* **14**, 99 (1986). Intense and widespread potassium feldspar alteration appears to require regional fluid migration [P. P. Hearn, J. F. Sutter, H. E. Belkin, *Geochim. Cosmochim. Acta* **51**, 1323 (1987)]. Others have suggested cross-basin hydrologic flow as an alternate to Oliver's squeegee hypothesis, for example, D. L. Leach and E. L. Rowan, *Geology* **14**, 931 (1986).
66. For an excellent review, see C. McCabe and R. D. Elmore, *Rev. Geophys.* **27**, 471 (1989).
67. W. S. Fyfe and R. Kerrich, *Chem. Geol.* **49**, 353 (1985).
68. T. Torgersen and W. B. Clark, *Geochim. Cosmochim. Acta* **49**, 1211 (1985); T. Torgersen *et al.*, *Earth Planet Sci. Lett.* **92**, 43 (1989).
69. J. W. Hedenquist and R. W. Henley, *Econ. Geol.* **80**, 1640 (1985), and other articles in this special issue on ore-hosted breccias.
70. M. K. Hubbert and W. W. Ruby, *Geol. Soc. Am. Bull.* **70**, 115 (1959).
71. R. H. Sibson, in *Earthquake Prediction: An International Review*, D. W. Simpson and P. G. Richards, Eds. (Maurice Ewing Series, American Geophysical Union, Washington, DC, 1981), pp. 593–603.
72. G. J. Demaison, *Am. Assoc. Pet. Geol. Bull.* **61**, 1950 (1977).
73. A. E. Williams and M. A. McKibben, *Geochim. Cosmochim. Acta* **53**, 1905 (1989).
74. A. M. Bateman, *Economic Mineral Deposits* (Wiley, New York, 1942).
75. J. Toth, in (*15*), pp. 485–502; J. M. Sharp and J. R. Kyle, *ibid.*, pp. 461–483; C. M. Bethke, W. J. Harrison, C. Upson, S. P. Altaner, *Science* **239**, 261 (1988).
76. C. K. Paull and A. C. Neumann, *Geology* **15**, 545 (1987).
77. I thank D. Chapman, C. Forster, J. Hunt, J. Oliver, T. Torgersen, and J. Whelan for reviews and useful suggestions, and W. Hallager and coauthors for permission to cite their article in press in *Geology* and R. Henley, P. Roberts, and J. Hedenquist for organizing the 1983 field conference at which the cover photo was taken. Research support bearing on the topics discussed was provided by the Gas Research Institute, the Petroleum Research Fund, and eight company sponsors of the Global Basins Research Network.

Fluid Processes in Subduction Zones

SIMON M. PEACOCK

Fluids play a critical role in subduction zones and arc magmatism. At shallow levels in subduction zones (<40 kilometers depth), expulsion of large volumes of pore waters and CH_4-H_2O fluids produced by diagenetic and low-grade metamorphic reactions affect the thermal and rheological evolution of the accretionary prism and provide nutrients for deep-sea biological communities. At greater depths, H_2O and CO_2 released by metamorphic reactions in the subducting oceanic crust may alter the bulk composition in the overlying mantle wedge and trigger partial melting reactions. The location and consequences of fluid production in subduction zones can be constrained by consideration of phase diagrams for relevant bulk compositions in conjunction with fluid and rock pressure-temperature-time paths predicted by numerical heat-transfer models. Partial melting of subducting, amphibole-bearing oceanic crust is predicted only within several tens of million years of the initiation of subduction in young oceanic lithosphere. In cooler subduction zones, partial melting appears to occur primarily in the overlying mantle wedge as a result of fluid infiltration.

SUBDUCTION ZONES REPRESENT SITES WHERE OCEANIC lithosphere, capped by variably hydrated oceanic crust and sediments, is consumed into the mantle. Volcanism in the overriding oceanic or continental plate generally occurs where the depth to the subducting slab is 80 to >150 km (*1*). The generation of magmas and continental crust at convergent plate margins is intimately linked to the behavior of C-O-H fluids (*2*) at depth in subduction zones. Our understanding of processes that occur at depths of ~100 km in subduction zones is based on geologic studies

The author is in the Department of Geology, Arizona State University, Tempe, AZ 85287.

Table 1. Estimates of bound volatiles in subducted oceanic crust, sediments, and arc magmas. The volume of subducted components in oceanic crust is based on an average rate of oceanic ridge magmatism (which should equal the subduction rate) of 20 km^3 $year^{-1}$ (*3*), and a 2.5-km-thick basaltic layer and a 5-km-thick gabbroic layer. The volume of subducted sediments is for subduction of a 200-m-thick layer of pelagic sediments past the accretionary prism. The arc magmatism rate of 5 km^3 $year^{-1}$ falls within the reported range of 3 to 9 km^3 $year^{-1}$.

Volatile reservoir	Volume subducted or formed (km^3 $year^{-1}$)	Density (kg m^{-3})	Volatile contents (% by weight)		Mass subducted or formed (kg $year^{-1}$)	
			H_2O	CO_2	H_2O	CO_2
Pelagic sediment	0.53	2500	5	12	0.7×10^{11}	1.6×10^{11}
Oceanic crust						
Basalt	6.7	3000	2	0.1	4.0×10^{11}	0.2×10^{11}
Gabbro	13.3	3000	1	0.1	4.0×10^{11}	0.4×10^{11}
				Total subducted	8.7×10^{11}	2.2×10^{11}
Arc magmas	5.0	2700	1	0.05	1.4×10^{11}	6.8×10^{9}

of metamorphic and igneous rocks brought to the surface from great depth and indirect methods including laboratory experiments, computer modeling, and inverse geochemical and geophysical techniques. At shallow depths, <10 to 40 km, fluid processes in subduction zones are relatively well constrained by geological and geophysical (for example, seismic reflection) studies of active convergent plate margins and by geological studies of ancient subduction zones. Geologic samples from greater depths are rare and greater reliance must be placed on computer modeling combined with the results of experiments conducted at high pressures and temperatures. In this article, I review current hypotheses and evidence regarding the role that fluids (primarily H_2O) and fluid-bearing minerals (primarily hydrous silicates) play in subduction zones. In addition, I describe the evolution of fluids and the possible effects on arc magmatism using metamorphic rock and fluid pressure-temperature-time paths predicted by computer modeling.

Volatile Budget

Estimates of magma production rates and volatile contents allow comparison of the mass of volatiles subducted to the mass of volatiles present in arc magmas (Table 1), illustrate the scale of fluid involvement, and lead to several key questions regarding the role and significance of fluids in subduction zones. Currently, magmatism at ocean ridges forms ~20 km^3 of oceanic crust per year (*3*); a comparable amount of oceanic crust is subducted each year. The amount of volatiles subducted to mantle depths consists of two components: (i) volatiles stored in the oceanic crust and (ii) volatiles stored in sediments subducted past the accretionary wedge. Each component undergoes a different history in subduction zones and needs to be considered separately. Variable amounts of volatiles, primarily H_2O, are added to the basaltic oceanic crust at mid-ocean ridges during large-scale hydrothermal convection. Pelagic sediments, containing abundant CO_2 and H_2O in minerals, are deposited on the oceanic crust as it spreads away from the mid-ocean ridge. Magmatic fluxes have varied considerably over geologic time, and the volatile estimates have large uncertainties, but the estimates in Table 1 suggest that an order of magnitude more H_2O and CO_2 is subducted each year than may be accounted for in arc magmas.

Where is the remaining 90% of the subducted volatiles? Probable solutions include: (i) volatiles exsolve and escape from arc magmas during volcanism and plutonism; (ii) metamorphic reactions release volatiles from the subducting slab that migrate up along the subduction shear zone and ultimately reach the surface; (iii) volatiles released by metamorphic reactions are incorporated into the overlying mantle wedge via hydration and carbonation reactions; (iv) the slab does not completely devolatilize, and CO_2- and H_2O-bearing oceanic crust returns to the deep mantle (>200 km); and (v) some volatile-bearing magmas do not reach crustal levels. Field studies of active and ancient convergent plate margins clearly demonstrate that processes (i), (ii), and (iii) occur to some degree; processes (iv) and (v) may occur, but are not required by mass balance constraints because of the large uncertainties in the volatile estimates.

Fluids in oceanic crust. The primary source of H_2O in subduction zones at magma genesis depths is the breakdown of hydrous minerals contained in the basaltic, gabbroic, and ultramafic layers of the oceanic crust. Unaltered basalt samples indicate that magmas derived from upwelling asthenosphere beneath mid-ocean ridges contain only minor amounts of volatiles, ~0.15 to 0.40% H_2O (by weight) and <400 ppm CO_2 (*4*). Hydrous minerals, mainly prehnite, chlorite, amphibole, and serpentine, form in the oceanic crust as a result of hydrothermal circulation and metamorphism under conditions of high temperature and low pressure at mid-ocean ridges (*5*). Water is also added to the oceanic crust by the formation of zeolites and clay minerals during low temperature alteration and submarine weathering (*6*). Hydrous minerals are not distributed homogeneously throughout the oceanic crust (*7*), but rather occur preferentially in, and adjacent to, fractures and permeable zones.

The amount of H_2O and CO_2 in altered oceanic crust generally decreases downward, but the depth of alteration remains uncertain. Estimates of the volatile content of oceanic crust come from drill cores, dredge hauls, and ophiolites (fragments of probable oceanic crust that have been incorporated into continental crust). Relatively few drill holes have penetrated the crystalline oceanic crust; to date, the deepest drill hole (DSDP Site 504B) penetrated only ~1 km into basalt (*8*). Based on chemical analyses of drill cores of oceanic crust (*8*), I estimate that the 2.5-km-thick basaltic layer contains ~2% H_2O and ~0.1% CO_2 (by weight) bound in minerals (Table 1).

Samples of the deeper oceanic gabbro layer include rare drill cores and rocks from dredge hauls from oceanic fracture zones that may have higher average volatile contents than typical oceanic crust. Ophiolites have undergone a complex emplacement history and generally are not representative of oceanic crust formed at mid-ocean ridges (*9*). The $^{18}O/^{16}O$ ratios of gabbroic rocks exposed in ophiolites, such as the Oman ophiolite, suggest that the rocks have interacted extensively with fluids at high temperatures but without accompanying mineralogic alteration (*10*). Significant amounts of volatiles may have been added to the gabbros before complete crystallization by stoping and assimilation of overlying hydrated basalts (*10*). Based on the limited available data (*11*), I estimate that the 3- to 5-km-thick oceanic gabbro layer contains ~1% H_2O and ~0.1% CO_2 (by weight) (Table 1).

The volatile content of ultramafic rocks beneath the gabbro layer is poorly constrained, and the only direct samples are from ophiolites and samples dredged from fault scarps, which may also not be representative of the oceanic crust as a whole. Some H_2O may be

present as serpentine or talc in the ultramafic layer of the oceanic crust, but because of the unknown extent and depth of hydration, a volatile estimate is not included for ultramafic rocks in Table 1.

Fluids in overlying pelagic sediments. As cooling oceanic lithosphere spreads away from the mid-ocean ridge, pelagic (deep-sea) sediments are deposited on the oceanic crust. The primary source of CO_2 in subduction zones is the breakdown of carbonate minerals in pelagic sediments (Table 1). The total mass of pelagic sediment on the ocean floor is estimated at $\sim 1.4 \times 10^{20}$ kg (*12*) and consists of approximately 72% carbonate ooze, 19% red clay, and 9% siliceous ooze by volume (*13*). For a given area, the relative proportion of these sediments depends on several factors including the age of the oceanic crust, the depth to the ocean floor (a function of time), latitude, and the proximity of islands and continental land masses (*14*). Over geologic time, the evolution and abundance of marine species, such as calcareous plankton, have also affected the composition of pelagic sediments. Thus, different subduction zones may have significantly different pelagic sediment inputs and therefore different volatile inputs.

Average pelagic sediments contain approximately 12% CO_2 and 5% H_2O (by weight) bound in mineral structures (*15*) plus up to 50% H_2O (by volume) in pore spaces. Roughly $\sim 2 \times 10^{11}$ kg of bound H_2O and $\sim 4 \times 10^{11}$ kg of CO_2 would be subducted each year in pelagic sediments if a 200-m-thick column of sediments is subducted past the accretionary prism (Table 1).

Accretionary Prisms

In some subduction zones, such as the Lesser Antilles, much of the oceanic sediments and the contained fluids are removed by offscraping and underplating in accretionary prisms that form on the overriding plate adjacent to the trench (*16*). In other subduction zones, such as the Marianas and Japan trenches, little or no sediment accretion occurs (*17, 18*). Thus, different subduction zones differ greatly in the amount of sedimentary material removed at the accretionary prism, but in many cases at least some sediment and bound fluids appear to be subducted to deeper levels. For example, a seismic reflection study of the Barbados accretionary prism clearly images offscraping of the upper 250 m of the 1-km-thick sedimentary column entering the subduction zone (*19*); additional sedimentary material is underplated onto the base of the accretionary prism as the oceanic plate descends beneath the prism, but some sediments appear to be subducted past the accretionary prism (*19*). Oceanward of the Japan trench, new and reactivated normal faults, caused by the bending of the oceanic lithosphere, form structural basins that can trap sediments and promote their subduction (*18, 20*). On the basis of a mechanical model of subduction zones, Shreve and Cloos showed that the amount of sediment subducted depends on the subduction zone geometry, the subduction rate, the sediment input rate, and the physical properties of the sediments and overriding plate (*21*); their model predicts that at least some oceanic sediments are subducted to depths greater than 100 km. In the Alpine collision zone, the presence of coesite in high-pressure metasedimentary rocks requires that sedimentary material was subducted to depths greater than 90 km (*22*). Most accretionary prisms consist of terrigenous sediments derived from nearby island arcs and continental land masses, lesser amounts of pelagic sediments, and minor basaltic and ultramafic rocks. Terrigenous sediments occur above, and are less lithified than, underlying pelagic sediments (*23*); terrigenous sediments, therefore, are more likely to be incorporated in an accretionary prism, and avoid subduction, as compared to pelagic sediments. Essentially all oceanic crust is subducted past the accretionary prism.

In general, the amount of fluids released during subduction decreases with depth. As pelagic sediments are dragged beneath the accretionary prism, compaction and lithification results in the expulsion of large amounts of pore fluids (*24*). Sediment porosities range from 10 to 50% whereas low-grade metasedimentary rocks have porosities of <5 to 10% (*24*). Observations of active accretionary prisms (Japan, Barbados, Oregon-Washington, Marianas) have yielded abundant evidence of pore fluid expulsion, including the presence of biological communities, temperature and geochemical anomalies, mud volcanos and diapirs, and actual fluid vents (*25*).

Estimates of fluid fluxes out of accretionary prisms, based on heat transfer calculations and direct measurements, range from 10^{-3} to 10^{-2} m^3 m^{-2} year^{-1} over broad regions to >50 m^3 m^{-2} year^{-1} in local vents (*25*). The results of deep-sea drilling and submersible investigations strongly suggest that fluid flow is focused along faults, fractures, and permeable horizons (*25*). The presence of thermogenic methane in expelled fluids requires that fluids that formed at temperatures >60°C and depths >3 km (and thus tens of kilometers from the trench) are tapped by the fluid flow system of the accretionary prism (*25*). Cloos (*26*) interpreted landward-dipping seismic reflections in modern accretionary prisms as possibly representing active dewatering conduits.

Increases in pressure and temperature drive diagenetic and low-grade metamorphic devolatilization reactions in subducted sediments and oceanic crust. The transformation of opal-A, the main component of siliceous oozes, to quartz during diagenesis releases approximately 5 to 10% H_2O (by weight) (*27*). Clay minerals begin to break down and release H_2O at temperatures of 50° to >150°C (*28*). Thermogenic methane is produced by the breakdown of hydrocarbons at temperatures of ~60° to 150°C (*29*). At low temperatures the breakdown of hydrocarbons, clay minerals, and carbonates will produce C-O-H fluids (*30*). Below ~350°C, separate CH_4-rich and H_2O-rich fluids appear to coexist as evidenced by experiments and the presence of separate H_2O-rich and CH_4-rich fluid inclusions in high-pressure metasedimentary rocks (*30, 31*). At higher temperatures and oxygen fugacities, miscible CO_2-H_2O fluids are stable (*32*).

Two additional processes that appear to occur beneath the accretionary prism are (i) redistribution of H_2O in the subducting oceanic crust and (ii) possible addition of H_2O to the oceanic crust (*33*). Exposed basalts that were metamorphosed under blueschist-facies (high-pressure, low-temperature) conditions have relatively

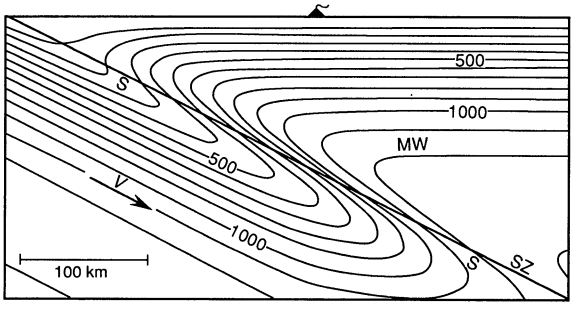

Fig. 1. Thermal structure of a subduction zone after 10 million years of subduction predicted by a numerical, two-dimensional heat transfer model (*38*). Contour interval is 100°C. For this calculation, a 27° subduction zone was formed in 50-million-year-old oceanic crust. The convergence rate (v) is 3 cm year^{-1}, there is no shear heating, and there is no induced convection in the overlying mantle wedge. The thermal structure of a subduction zone evolves with time. Numerical experiments can be used to predict pressure-temperature-time (P-T-t) paths for rocks in subducting oceanic crust (the top 7.5 km of the slab, S) and the overlying mantle wedge (MW) as a function of different subduction parameters; SZ, shear zone separating the slab from the mantle wedge.

uniform mineralogies and H_2O contents in contrast to the heterogeneous distribution of hydrous minerals and H_2O in basalts altered at the mid-ocean ridge. This observation suggests that H_2O may be redistributed in the oceanic crust by local, contemporaneous dehydration and hydration reactions. Blueschists contain an average of ~3% H_2O (by weight) (*34*), slightly higher than the analyses of altered oceanic crust (Table 1); thus, additional hydration of oceanic crust may occur at shallow depths in subduction zones. The source of the additional H_2O may be fluids stored in pores or fractures, diagenetic dehydration reactions occurring in the overlying sediments, or dehydration reactions occurring at deeper levels in the subduction zone.

High-Pressure, Low-Temperature Metamorphism

Increases in pressure and temperature, accompanying continued subduction of oceanic crust and sediments into the mantle, drive additional devolatilization reactions that reduce the fluid content of the subducting slab. Surficial heat flow measurements and thermal models demonstrate that subduction of oceanic lithosphere tends to cool the surrounding mantle (*35*) (Fig. 1). Compared to rocks metamorphosed during continent collision or magma intrusion, rocks in subduction zones are metamorphosed at relatively high pressures and low temperatures. Metamorphic dehydration reactions in subducting slabs have been previously investigated by superposing petrogenetic grids onto representative thermal structures of subduction zones (*36, 37*). In this article, I take an alternative approach and use two-dimensional numerical models of heat transfer in subduction zones to predict specific P-T-t paths for rocks in the subducting slab and the overlying mantle wedge (*38*) (Fig. 2). Such P-T-t paths can be used to predict the temporal evolution of fluids and the effects of various parameters. The P-T-t paths followed by the subducting slab govern the nature and location of metamorphic and partial melting reactions in subducted oceanic crust and sediments, the composition and amount of fluids produced, and fluid fluxes as a function of time and space. Similarly, P-T-t paths followed by rocks in the overlying mantle wedge determine the effects of fluid infiltration and location of partial melting reactions. Possible fluid P-T-t paths are also predicted by the numerical model (*38–40*).

Subduction zone P-T-t depend on numerous variables that differ for each subduction zone. Numerical experiments demonstrate that among the most important factors are the age of the incoming oceanic lithosphere, the amount of previously subducted lithosphere, the location of the rock in the subduction zone, and the vigor of convection in the mantle wedge induced by the subducting slab (Fig. 2). Subduction zones that form in young, relatively hot, oceanic lithosphere result in warmer slab P-T-t paths as compared to subduction zones that form in older oceanic lithosphere (Fig. 2A). For a given subduction zone, incoming oceanic crust and sediments

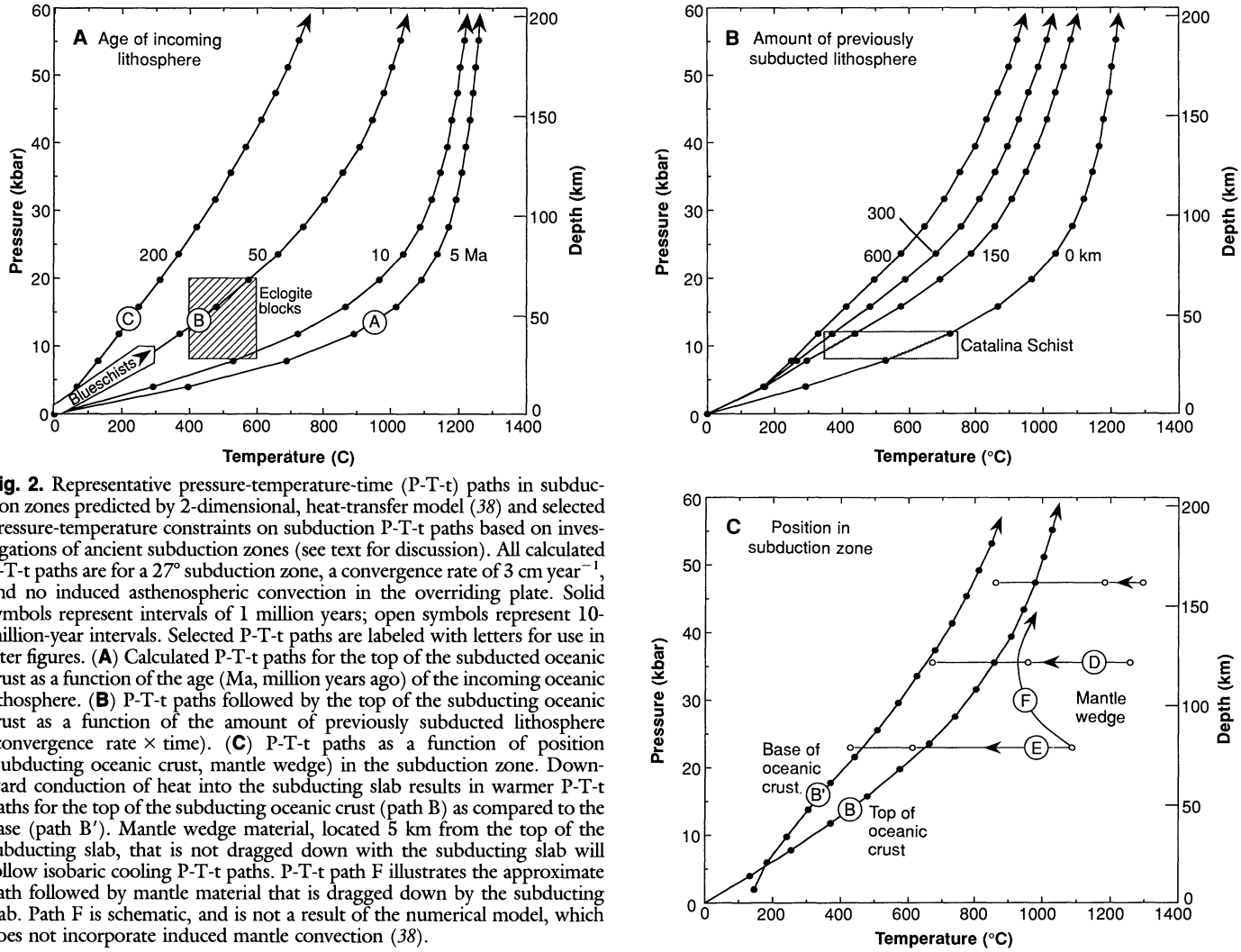

Fig. 2. Representative pressure-temperature-time (P-T-t) paths in subduction zones predicted by 2-dimensional, heat-transfer model (*38*) and selected pressure-temperature constraints on subduction P-T-t paths based on investigations of ancient subduction zones (see text for discussion). All calculated P-T-t paths are for a 27° subduction zone, a convergence rate of 3 cm year^{-1}, and no induced asthenospheric convection in the overriding plate. Solid symbols represent intervals of 1 million years; open symbols represent 10-million-year intervals. Selected P-T-t paths are labeled with letters for use in later figures. (**A**) Calculated P-T-t paths for the top of the subducted oceanic crust as a function of the age (Ma, million years ago) of the incoming oceanic lithosphere. (**B**) P-T-t paths followed by the top of the subducting oceanic crust as a function of the amount of previously subducted lithosphere (convergence rate × time). (**C**) P-T-t paths as a function of position (subducting oceanic crust, mantle wedge) in the subduction zone. Downward conduction of heat into the subducting slab results in warmer P-T-t paths for the top of the subducting oceanic crust (path B) as compared to the base (path B′). Mantle wedge material, located 5 km from the top of the subducting slab, that is not dragged down with the subducting slab will follow isobaric cooling P-T-t paths. P-T-t path F illustrates the approximate path followed by mantle material that is dragged down by the subducting slab. Path F is schematic, and is not a result of the numerical model, which does not incorporate induced mantle convection (*38*).

follow progressively cooler P-T-t paths as heat is advected from the system by subducting oceanic lithosphere (Fig. 2B). Qualitatively, P-T-t paths calculated for mature subduction zones resemble P-T-t paths calculated for subduction zones developed in older oceanic lithosphere. Conduction of heat downward from the overlying mantle wedge into the top of the subducting slab results in warmer P-T-t paths for the top of the oceanic crust as compared to the base (Fig. 2C). In subduction zones where induced asthenospheric convection in the overriding plate is insignificant, the overlying mantle wedge cools with time (Fig. 2C). In subduction zones with induced asthenospheric convection, rocks in the mantle wedge near the subducting slab will first cool, and then heat up as they are dragged downward. Induced asthenospheric convection will act to retard the overall cooling of a subduction zone (*41*).

Additional processes, such as shear heating (frictional heating, viscous dissipation) and metamorphic reactions, affect subduction zone P-T-t paths, but only to a minor extent. The thermal effect of shear heating is proportional to the shear stress in the subduction shear zone. In numerical experiments that incorporate shear heating, at a maximum shear stress of 250 bars (*42*), calculated slab P-T-t paths are only 50°C warmer than in calculations in which frictional heating is neglected (*43*). Incorporation of endothermic, prograde metamorphic reactions in the subducting slab result in calculated P-T-t paths that are only 5°C cooler (*43*).

Metamorphic rocks preserved in ancient subduction zones serve as critical tests of the reliability of calculated P-T-t paths (Fig. 2). P-T-t paths calculated for subduction zones (Fig. 2A) are consistent with P-T paths deduced for blueschist-facies (high pressure, low temperature) metamorphic rocks (*44*) and P-T estimates for high-grade eclogite blocks found in subduction melanges (*45*). The inverted metamorphic gradient preserved in the Catalina Schist terrane of southern California records progressive underplating during cooling from ~750° to ~350°C at pressures of ~10 kbar (*39, 46, 47*). This record is consistent with the cooling with time predicted for a given subduction zone (Fig. 2B). Subduction zone cooling is also consistent with the observation that eclogite blocks, such as occur in the Franciscan Formation of California, typically record the highest temperatures and the oldest (earliest) radiometric ages for a given subduction zone (*45*). The Central Metamorphic Belt in northern California records an apparent inverted thermal gradient developed in subducted oceanic crust (*39, 48*) consistent with the conduction of heat downward from the mantle wedge into the top of the subducting slab (Fig. 2C). The good agreement between the field data and predicted P-T-t paths at shallow depths suggests that these thermal models are reasonable and can be used to predict P-T-t paths and fluid processes at greater depths.

Prograde metamorphism of subducted clay-rich pelagic sediments and the release of fluids can be modeled with the Al_2O_3-SiO_2-H_2O (ASH) system. As shown in Fig. 3, the sequence of reactions encountered by subducting clay-rich sediments depends on the P-T-t path followed by the top of the subducting slab. For a rock consisting of 1:1 volume mixture of quartz and kaolinite, the first reaction encountered in cool subduction zones (path C, Fig. 3) will be the breakdown of kaolinite to quartz + diaspore + H_2O; this reaction releases 90 kg of H_2O per cubic meter of rock (Fig. 4). In cool subduction zones, the second reaction, diaspore + quartz → kyanite + H_2O, may be encountered at ~450°C and 30 to 40 kbar; it releases an additional 90 kg of H_2O per cubic meter of rock. This second reaction occurs at magma genesis depths and thus dehydration of diaspore may be an important source of H_2O in mature subduction zones where large amounts of clay-rich pelagic sediments are subducted (*49*).

The limitations of this theoretical approach point out critical research areas. First, the petrogenetic grid was extrapolated from thermodynamic data for minerals obtained at pressures less than 10 kbar (*50*). Uncertainties in the location of reactions at higher pressures are large. More importantly, this approach does not consider possible ASH minerals that may be stable at high pressures. Numerous high-pressure phases have been discovered in experiments conducted in the MgO-SiO_2-H_2O system (*51*), and thus additional high-pressure ASH phases are also likely. Secondly, the ASH system only approximates the composition of clay-rich pelagic sediments. A better approximation would include the additional components CaO, CO_2, and Fe_2O_3. Possible important volatile-bearing minerals in the expanded chemical system include aragonite, calcite, clinozoisite, epidote, laumonite, lawsonite, margarite, meionite, prehnite, waikarite, yugowaralite, and zoisite. The inclusion of CO_2 results in the necessity of considering mixed-volatile equilibria and the effects of fluid infiltration on reaction progress. A probable miscibility gap in the H_2O-CO_2 system at high pressures and low temperatures is an added complication (*32*). In addition to forming new minerals, inclusion of Fe_2O_3 results in solid solutions in several phases, such as epidote, $Ca_2Al_2(AlFe^{3+})Si_3O_{12}(OH)_2$. In order to model fluid production, accurate solution models are needed for all phases exhibiting solid solutions. The oxygen fugacity of the subducting sediments will determine the oxidation state of iron, and therefore which Fe-bearing phases are stable, as well as determining the speciation of evolved fluids.

Hydrous silicates present in sedimentary rocks metamorphosed under blueschist-facies conditions include phengite, glaucophane, chlorite, lawsonite, and stilpnomelane. At 300°C, aragonite is the stable $CaCO_3$ polymorph at pressures greater than ~7 kbar (*52*). Samples of sedimentary rock metamorphosed at pressures greater than 10 kbar are extremely rare. The hydrous minerals talc, phengite, glaucophane, ellenbergerite, Mg-Fe carpholite, and Mg-chlorrotoid occur in coesite-bearing metasedimentary rocks from the Alps that were metamorphosed at pressures ≥28 kbar during continent collision (*22*).

Modeling the fluid production of subducting basaltic oceanic crust is difficult because of its chemical complexity. Basalts consist of nine major chemical components, K_2O, Na_2O, CaO, MgO, FeO, Fe_2O_3, Al_2O_3, SiO_2, and H_2O, plus several important minor

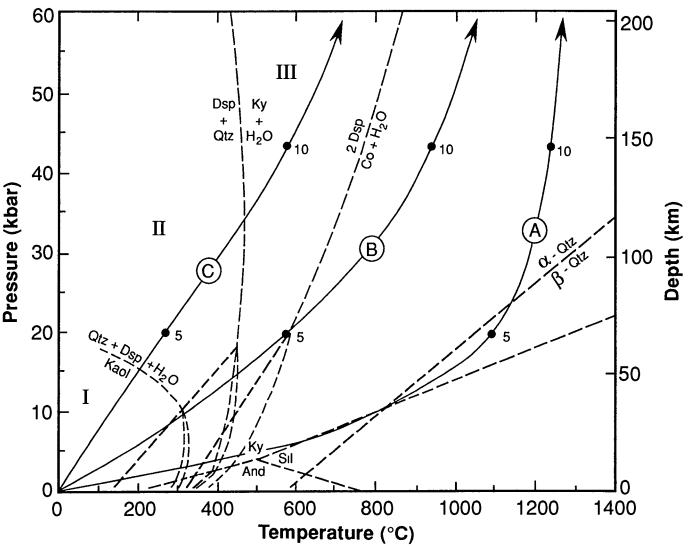

Fig. 3. Reactions in the Al_2O_3-SiO_2-H_2O system (dashed lines) predicted from thermodynamic data (*50*). And, andalusite; Co, corundum; Dsp, diaspore; Kaol, kaolinite; Ky, kyanite; Qtz, quartz; Sil, sillimanite. Different dehydration reactions are encountered for different P-T-t paths (solid lines). Numbers indicate time in millions of years along each path (see Fig. 2).

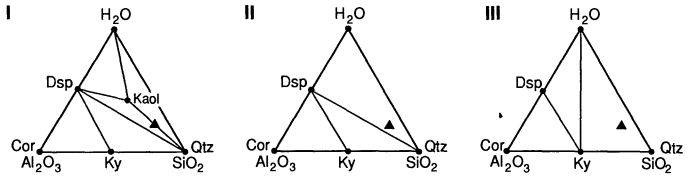

Fig. 4. Ternary diagrams illustrating phase topology for three different P-T regions (I, II, and III) encountered by P-T-t path C in Fig. 3. Numbers beneath ternary diagrams represent masses of each phase per cubic meter of initial sediment, assuming no fluids leave the system. In real subduction zones, fluids produced by devolatilization reactions will escape. (**Left**) Initial bulk composition (solid triangle) representing a 1:1 volumetric mixture of quartz and kaolinite. (**Center**) The reaction Kaol = Dsp + Qtz + H_2O releases 90 kg of H_2O per m^3. (**Right**) The reaction Dsp + Qtz = Ky + H_2O releases an additional 90 kg of H_2O per m^3. Fluids released by the breakdown of diaspore may be a significant source of H_2O in cool subduction zones at magma genesis depths.

components, MnO, TiO_2, and CO_2. Important hydrous minerals, such as amphibole, mica, and chlorite, exhibit complex solid solutions that are functions of pressure, temperature, oxygen fugacity, and bulk composition.

The complex phase relations of metabasalts have been elucidated at pressures less than 10 kbar (~35 km) (*53*), but few subsolidus experiments have been performed in basaltic bulk compositions at pressures between 10 and 50 kbar. We have only limited knowledge of basaltic phase relations at P-T conditions appropriate for subducted oceanic crust and thus predicting fluid production in subducting oceanic crust is speculative. Most of our current understanding of subduction zone metamorphism of basalt comes from the study of rocks in ancient subduction zones, such as the Franciscan Complex in California. Diagnostic minerals developed in metabasalt under high-pressure, low-temperature conditions include pyrope and jadeite, and the hydrous minerals glaucophane, lawsonite, and phengite (*54*). Amphiboles of varying composition are stable in metabasalts over a wide range of P-T conditions; sodic amphibole is probably an important H_2O reservoir in subducted oceanic crust. If the ultramafic layer of the oceanic crust is substantially hydrated at the mid-ocean ridge or beneath the accretionary prism, then serpentine and talc will also be important H_2O reservoirs in subducting slabs.

In relatively warm subduction zones, developed in young oceanic lithosphere (path A, Fig. 5), subducting slab P-T-t paths intersect the wet solidus at pressures of 10 to 28 kbar. The amount of H_2O present in the rock as a free fluid phase will determine the amount of melt generated. The porosity of metabasalt at high pressures is unknown, but probably low (~0.1% or less). Unless subducting oceanic crust is infiltrated by substantial amounts of H_2O produced by dehydration reactions in rocks located upstream, only a small amount of partial melt should form. At pressures <28 kbar metabasalt will contain hornblende. When the rock crosses the HBL OUT curve (Fig. 5), fluid-absent partial melting occurs associated with the breakdown of hornblende. Any H_2O bound in the hornblende crystal lattice partitions directly into the partial melt, without forming a separate aqueous fluid.

The P-T-t paths calculated for cool subduction zones (path C, Fig. 5) do not intersect the wet basalt solidus at pressures <50 kbar; these relations suggest that melting of oceanic crust is an unlikely source of arc magmas in mature subduction zones or subduction zones that form in old oceanic lithosphere. Whether hydrous minerals are stable in metabasaltic compositions at pressures of 30 to 50 kbar remains a major unresolved question. If hydrous minerals are stable, then H_2O may be subducted into the deep mantle past the source region of arc magmas. If hydrous minerals are not stable, then complete dehydration of subducted oceanic crust will provide a source of H_2O fluids that may trigger melting in overlying rocks. The generation of pore fluids during dehydration reactions reduces the effective stress on the rock and promotes brittle failure (*55*); serpentine dehydration has been proposed as a possible triggering mechanism for deep (>300 km) earthquakes (*56*).

Numerical models predict that the base of the hydrated oceanic crust will dehydrate last for a temperature-sensitive dehydration reaction, such as the breakdown of tremolite (Fig. 5). During early subduction, fluids released from deep levels flow up temperature if they flow toward the subduction shear zone because of the temperature inversion present at the top of the subducting slab. Thus, fluids may trigger melting in the overlying oceanic crust if the temperature there exceeds the wet solidus. For example, consider P-T-t paths B and B′ (Fig. 5), which represent conditions encountered during subduction by the top and base of the subducting oceanic crust, respectively. If the tremolite breakdown reaction is used as a model, the top of the oceanic crust will dehydrate at ~28 kbar. The dehydration front will move downward with time until the base of the oceanic crust dehydrates at ~34 kbar. As H_2O flows upward, it will encounter anhydrous oceanic crust at temperatures above the wet solidus and trigger fluid-present partial melting in the top of the oceanic crust. In cooler subduction zones, possible fluid P-T-t paths through subducting oceanic crust do not cross the wet basaltic solidus, and partial melting of the slab is not predicted.

In a subduction zone, hydrous minerals are concentrated in the basaltic oceanic crust whereas carbonates are concentrated in overlying pelagic sediments. Upward flow of H_2O-rich fluids released by dehydration reactions in the oceanic crust may drive decarbonation

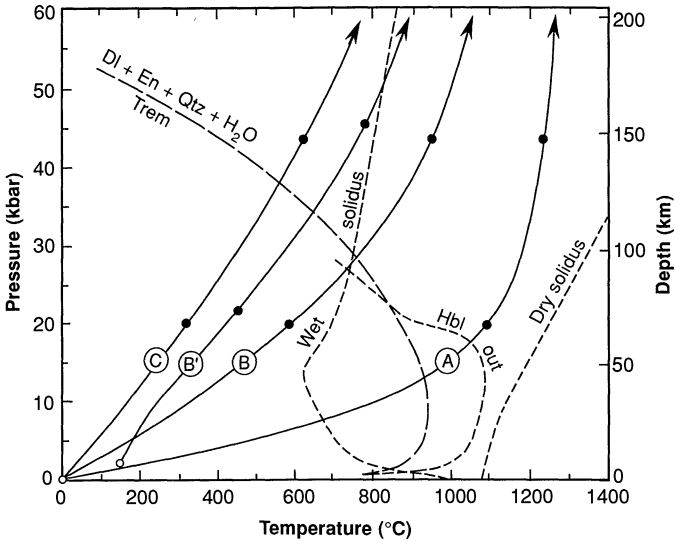

Fig. 5. Representative P-T-t paths (solid lines) and experimental melting relations (short dashed lines) for the basalt + H_2O system (*65*). The addition of excess H_2O drastically decreases the melting temperature of basalt (compare dry versus wet solidi). Hbl out curve represents fluid-absent partial melting of hornblende-bearing metabasalt. Long dashed line represents calculated tremolite dehydration reaction (*50*), which is similar to the stability field of chemically complex amphiboles synthesized experimentally (*66*). Subducted oceanic crust following P-T-t paths cooler than path B will dehydrate before reaching melting reactions; this relation suggests that arc magmas in cool subduction zones are not derived from partial melting of the oceanic crust. Warmer P-T-t paths predicted for subduction zones developed in young oceanic lithosphere result in substantial partial melting associated with the breakdown of hornblende at pressures less than ~28 kbar.

reactions in the overlying pelagic sediments (*57*).

Fluids released by devolatilization reactions will tend to migrate upward because H_2O and CO_2 fluids are one half to one third as dense as rock under subduction zone conditions. Fluid flow, like all advective heat-transfer mechanisms, essentially translates the thermal structure from upstream to downstream areas. In a subduction zone, inverted thermal gradients occur at the slab-mantle interface (Fig. 1). Fluids migrating upward from the cooler, subducting slab into the warmer, overlying mantle will tend to cool the overlying mantle. Fluids migrating up along the subduction shear zone will travel down thermal gradients and therefore tend to warm rocks in the shear zone. The magnitude of the thermal perturbation caused by fluid flow is proportional to the thermal gradient along the fluid flow path and the volumetric fluid flux (the volume of fluid passing through a cross-sectional area per time). As discussed above, most pore fluids will be expelled at depths of <10 to 40 km. At greater depths devolatilization reactions provide the only source of fluids, and fluid fluxes should be much lower than those observed in accretionary prisms. Numerical models of metamorphic reactions suggest vertical fluid fluxes out of subducting oceanic crust range from a maximum of 10^{-3} m^3 m^{-2} $year^{-1}$ associated with discontinuous dehydration reactions to less than 10^{-4} m^3 m^{-2} $year^{-1}$ for continuous dehydration reactions (*40, 58*). Heat transfer calculations indicate that the thermal effect of these fluid fluxes are minor (*40, 58*). The thermal structure of subduction zones at depths >40 km is controlled primarily by heat conduction and the advection of heat by subducting oceanic lithosphere; heat advection by fluid flow is relatively insignificant.

Fluid Infiltration and Partial Melting of the Mantle Wedge

Investigations of active and ancient subduction zones demonstrate that at least some of the fluids released from the subducting slab migrate upward into the overlying mantle wedge. Serpentinite diapirs present in the Marianas forearc appear to result from hydration of the mantle wedge above the subducting slab (*59*). In the Trinity thrust system (northern California) and the Catalina Schist terrane (southern California), fluids derived from subducted basalt and sediments reacted with the mantle wedge to form carbonates and hydrous silicates, such as serpentine, talc, and Mg-amphibole, at pressures of 5 to 10 kbar (*47, 60*). The infiltrating H_2O-CO_2 fluids also carried dissolved chemical species, such as SiO_2 and CaO, that were added to the mantle wedge, thereby changing its bulk composition (*47, 60*). At deeper levels in subduction zones similar hydration, carbonation, and metasomatic processes should occur in the mantle wedge above devolatilization reaction sites in the subducting slab.

Predicting the consequences of fluid infiltration at depths >50 km requires knowledge of the phase equilibria, dynamic processes, and P-T-t paths appropriate for the mantle wedge. Several possible P-T-t paths are illustrated in Fig. 6, which shows selected phase equilibria for the system peridotite ± H_2O. For P-T-t path D (Fig. 6), H_2O infiltration at temperatures greater than the phlogopite-out curve will trigger partial melting of peridotite. However, when subduction begins the mantle wedge cools substantially before hydrous oceanic crust reaches 125 km depth. Fluids infiltrating the mantle wedge at temperatures below 1200°C will react with peridotite to form phlogopite, subject to the amount of K_2O and H_2O available in the rock and fluid. After all possible phlogopite has been formed, further H_2O infiltration will either (i) trigger fluid-present partial melting at temperatures above the wet solidus (>900°C) or (ii) not react with the rock (at 900° to 700°C) unless an additional hydrous phase is stable in the peridotite + H_2O system. In case (ii), fluid will continue to flow upward until it encounters mantle with unreacted K_2O, such that phlogopite may form, or reaches shallow pressures where hornblende forms. With time, a metasomatic front, defined by the formation of phlogopite, will migrate upward in the mantle until the front reaches pressure-temperature conditions above the wet solidus where fluid-present partial melting will occur.

For P-T-t path E (Fig. 6), H_2O infiltration at temperatures greater than 850°C will form amphibole and phlogopite; fluid-present partial melting will occur only after the capacity of the rock to form hornblende and phlogopite has been exceeded. Mantle wedge material that is dragged down with the subducting slab (P-T-t path F, Fig. 6) may undergo hydration first and then partial melting at deeper levels as the P-T-t path crosses the fluid-absent, hornblende- and phlogopite-out melting reactions (*61*). The extent to which induced convection of the mantle wedge occurs depends in part on the unknown rheology of hydrated mantle at depth. At temperatures less than 700°C, experiments demonstrate that talc is the stable hydrous phase that coexists with forsterite + enstatite in the MgO-SiO_2-H_2O system (Fig. 6). Once enstatite is converted to talc by hydration, further H_2O infiltration should stabilize serpentine at temperatures less than ~600°C. The calculated stability field of tremolite and the location of the experimentally determined, fluid-absent hornblende-melting curve suggest that amphibole may be stable in hydrated peridotite at pressures less than ~30 kbar. An understanding of the composition and stability field of amphibole in the mantle wedge awaits subsolidus experiments in the peridotite + H_2O system.

Geochemical evidence indicates that there is a direct chemical connection between the subducted slab and magmas formed at selected convergent plate margins. The radiogenic isotopic and trace

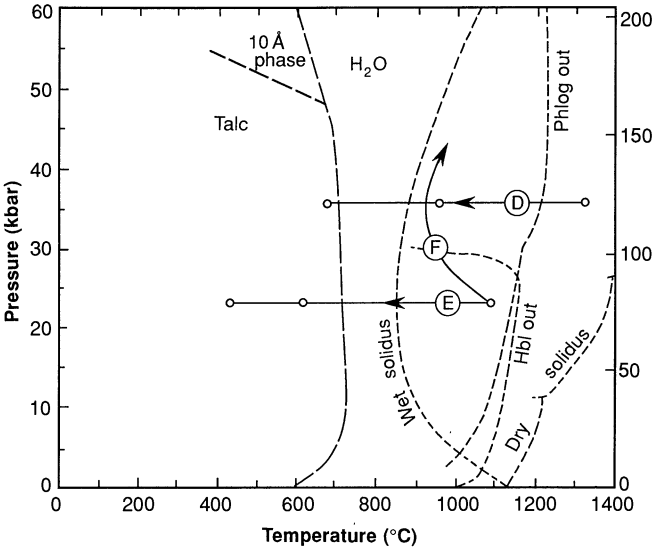

Fig. 6. Experimental partial-melting (short dashed lines) and subsolidus phase relations (long dashed lines) applicable to the peridotite + H_2O system (*67, 68*). As in the basalt system, the presence of excess H_2O decreases the melting temperature of peridotite. Chemically-complex amphibole and phlogopite are stable on the solidus up to ~30 kbar and >50 kbar, respectively. Hbl out and Phlog out curves represent fluid-absent partial melting of hornblende-bearing and phlogopite-bearing peridotite, respectively. Minerals associated with subsolidus reactions represent the stable hydrous phase that coexists with forsterite and enstatite in the simplified MgO-SiO_2-H_2O peridotite system (*68*). Thermodynamic calculations (*50*) suggest that serpentine may coexist with forsterite and enstatite at temperatures <600°C and pressures ≳20 kbar. P-T-t paths (solid lines) D and E represent isobaric cooling of the mantle wedge at 80 and 120 km depth, respectively. P-T-t path F represents P-T conditions encountered by mantle wedge that is dragged down with the subducting slab.

element systematics of some island arc volcanic rocks suggest that there is a contribution to arc magmas from subducted oceanic crust (*1, 62*). The recent discovery of elevated concentrations of ^{10}Be in lavas from the Japan, Aleutian, and Central American arcs has provided direct evidence of a young, subducted sedimentary component in arc magmas (*63*).

The question remains as to the physical nature of the slab component observed in arc magmas. The slab component may be carried by partial melts derived from subducted oceanic crust and sediment. Melting experiments at high pressures, however, appear to rule out the possibility that arc magmas are derived solely from partial melting of subducted oceanic crust (*64*). Alternatively, the slab component may be carried by low viscosity, H_2O-CO_2 fluids derived from devolatilization reactions in the subducted slab that migrated upward resulting in metasomatism and partial melting of the overlying mantle. If partial melting occurs solely within the mantle wedge, then infiltrating aqueous fluids must carry substantial amounts of silica, incompatible elements (for example, K_2O and TiO_2), and radiogenic components (for example, ^{87}Sr) in order to account for the composition of arc magmas (*1*).

Based on the model P-T-t paths discussed above, partial melting of subducting oceanic crust and sediments appear most likely to occur within a few tens of millions of years of the initiation of subduction in young oceanic lithosphere (<50 million years old). In more mature subduction zones and in subduction zones formed in older oceanic lithosphere, partial melting appears more likely to occur as a result of H_2O infiltration of the overlying mantle wedge. Fluids, whether present as a distinct volatile phase or bound in the crystal structure of minerals, play a crucial role in all subduction-zone partial melting scenarios.

REFERENCES AND NOTES

1. J. Gill, *Orogenic Andesites and Plate Tectonics* (Springer-Verlag, New York, 1981).
2. The term fluid is used to describe low viscosity C-O-H chemical species, such as H_2O, CO_2, and CH_4. Under most pressure-temperature conditions of subduction zones, these species are supercritical fluids possessing characteristics of both liquids and gases. In addition, CO_2 and H_2O may occur as dissolved species in magmas or bound in the crystal structure of minerals such as hydrous silicates, hydroxides, and carbonates.
3. J. A. Crisp, *J. Volcanol. Geotherm. Res.* **20**, 177 (1984); A. Reymer and G. Schubert, *Geology* **14**, 299 (1986).
4. G. Fine and E. Stolper, *Earth Planet. Sci. Lett.* 76, 263 (1986); J. E. Dixon, E. Stolper, J. R. Delaney, *ibid.* **90**, 87 (1988).
5. See, for example, A. Miyashiro, *Metamorphism and Metamorphic Belts* (Allen and Unwin, London, 1973); S. E. Humphris and G. Thompson, *Geochim. Cosmochim. Acta* **42**, 107 (1978); J. C. Alt and J. Honnorez, *Contrib. Mineral. Petrol.* **87**, 149 (1984).
6. J. Honnorez, in *The Sea*, C. Emiliani, Ed. (Wiley, New York, 1981), pp. 525–587.
7. J. C. Alt, J. Honnorez, C. Laverne, R. Emmermann, *J. Geophys. Res.* **91**, 10309 (1986).
8. Deep Sea Drilling Project (DSDP) hole 504B drilled 1100 m into 5.9-million-year-old rocks in the Cocos plate [R. N. Anderson *et al.*, *Nature* **300**, 589 (1982)]. Most analyses indicate that altered pillow basalts that form the upper part of the oceanic crust (0 to 600 m depth) contain between 0.5 and 1% H_2O and 0.1% CO_2 by weight (7). Lower sheeted dikes (600 to 1100 m depth) contain between 1 and 3% H_2O and between 0.05 and 0.1% CO_2 by weight (7). Alt *et al.* (7) specifically selected samples free of secondary veins for analysis; therefore, these values should be considered minimum estimates of the volatile content of the oceanic basaltic layer. DSDP holes 332B (in 3.5-million-year-old rocks from the Mid-Atlantic Ridge) and 418A (in 108-million-year-old rocks from the West Atlantic) penetrated >500 m of basalt. The H_2O content of 332B basalts generally increases downward, whereas the H_2O content of 418A basalts decreases downward; basalts from both holes contain an average of ~1% H_2O (by weight) [H. Staudigel, S. R. Hart, S. H. Richardson, *Earth Planet Sci. Lett.* **52**, 311 (1981)]. CO_2 contents are highly variable. Most 332B basalts contain <0.2% CO_2, whereas most 418A basalts contain >0.4% CO_2 by weight.
9. See, for example, R. C. Coleman, *Ophiolites* (Springer-Verlag, New York, 1977); papers in I. G. Gass, S. J. Lippard, A. W. Shelton, Eds., *Ophiolites and Oceanic Lithosphere* (Blackwell, Oxford, 1984).
10. R. T. Gregory and H. P. Taylor, Jr., *J. Geophys. Res.* **86**, 2737 (1981).
11. Variably deformed and hydrated gabbros recovered from Ocean Drilling Program (ODP) hole 735B (Atlantic II fracture zone) contain 0.79 ± 0.35% H_2O and 0.15 ± 0.10% CO_2 by weight [P. T. Robinson *et al.*, *Proc. Ocean Drilling Progr. Init. Rep.* **118**, 89 (1989)]. Twelve gabbroic samples from the Oman ophiolite lost an average of 2.3% volatiles by weight on ignition [J. D. Smewing, *J. Geophys. Res.* **86**, 2645 (1981)].
12. W. W. Hay, L. S. James, N. W. Christopher, *J. Geophys. Res.* **93**, 14933 (1988).
13. A. Poldevaart, *Geol. Soc. Am. Spec. Pap.* **62**, 119 (1955).
14. H. C. Jenkyns, in *Sedimentary Environments and Facies*, H. G. Reading, Ed. (Blackwell, Boston, ed. 2, 1986), pp. 343–397.
15. S. K. El Wakeel and J. R. Riley, *Geochim. Cosmochim. Acta* **25**, 110 (1961); A. B. Ronov and A. A. Yaroshevsky, *Trans. Geokhim.* **12**, 1761 (1976). Typical bound volatile contents of individual pelagic sediment types are: calcareous oozes, 23 to 30% CO_2, 3 to 4% H_2O; red clays and siliceous oozes, 1 to 3% CO_2, 6 to 7% H_2O by weight. All pelagic sediment types contain approximately 0.3% inorganic C by weight.
16. See, for example, G. K. Westbrook, *Geophys. J. R. Astron. Soc.* **43**, 201 (1975); J. C. Moore *et al.*, *Geol. Soc. Am. Bull.* **100**, 1578 (1988).
17. See, for example, D. M. Hussong and S. Uyeda, *Init. Rep. Deep Sea Drilling Proj.* **60**, 909 (1982).
18. J. P. Cadet *et al.*, *Earth Planet. Sci. Lett.* **83**, 267 (1987).
19. G. K. Westbrook *et al.*, *Geology* **16**, 631 (1988).
20. T. W. C. Hilde, *Tectonophysics* **99**, 381 (1983).
21. R. L. Shreve and M. Cloos, *J. Geophys. Res.* **91**, 10229 (1986); M. Cloos and R. L. Shreve, *Pure Appl. Geophys.* **128**, 455 (1988); *ibid.*, p. 501.
22. C. Chopin, *Contrib. Mineral. Petrol.* **86**, 107 (1984); W. Schreyer, *Fortschr. Mineral.* **63**, 227 (1985).
23. J. C. Moore, *Geology* **3**, 530 (1975).
24. C. J. Bray and D. E. Karig, *J. Geophys. Res.* **90**, 768 (1985).
25. The evidence for and consequences of fluid flow in accretionary prisms have been discussed by numerous investigators including M. W. Han and E. Seuss, *Eos* **57**, 1219 (1986); L. D. Kulm *et al.*, *Science* **231**, 561 (1986); J. Boulegue *et al.*, *Earth Planet, Sci. Lett.* **83**, 363 (1987); B. H. Reck, *J. Geophys. Res.* **92**, 3683 (1987); J. C. Moore and E. A. Silver, *Rev. Geophys.* **25**, 1305 (1987); A. Mascle *et al.*, Shipboard Scientific Party, *Proc. Ocean Drilling Prog., Int. Rep. Part A* **110**, 577 (1988); P. Henry, S. J. Lallemant, X. L. Pichon, S. E. Lallemand, *Tectonophysics* **160**, 277 (1989); M. G. Langseth and J. C. Moore, *Eos* **70**, 245 (1990).
26. M. Cloos, *Geology* **12**, 519 (1984).
27. See, for example, L. P. Knauth and S. Epstein, *Am. Mineral.* **67**, 510 (1982).
28. See, for example, J. Hower, in *Clays and the Resource Geologist*, F. J. Longstaffe, Ed. (Short Course 7, Mineralogical Association of Canada, Calgary, 1981), pp. 60–80.
29. G. E. Claypool and K. A. Kvenvolden, *Annu. Rev. Earth Planet. Sci.* **11**, 299 (1983).
30. J. R. Holloway, *Geology* **12**, 455 (1984).
31. L. C. Price, *Am. Assoc. Petrol. Geol. Bull.* **63**, 1527 (1979); P. Vrolijk, *Geology* **15**, 466 (1987); J. Mullis, in *Low Temperature Metamorphism*, M. Frey, Ed. (Chapman and Hall, New York, 1987), pp. 162–199.
32. J. R. Holloway, in *Fluid Inclusions*, L. S. Hollister and M. L. Crawford, Eds. (Short Course 6, Mineralogical Association of Canada, Calgary, 1981), pp. 13–38.
33. C. W. Burnham, in *Geochemistry of Hydrothermal Ore Deposits*, H. L. Barnes, Ed. (Wiley, New York, ed. 2, 1979), pp. 71–136.
34. W. G. Ernst, *J. Petrol.* **4**, 1 (1963); R. G. Coleman and D. E. Lee, *ibid.* **4**, 260 (1963).
35. Numerous thermal models of subduction zones have been presented in the literature, for example, E. R. Oxburgh and D. L. Turcotte, *Geol. Soc. Am. Bull.* **81**, 1665 (1970); K. Hasebe, N. Fuji, S. Uyeda, *Tectonophysics* **10**, 335 (1970); J. W. Minear and N. M. Toksoz, *J. Geophys. Res.* **75**, 1397 (1970); M. N. Toksoz, J. W. Minear, B. R. Julian, *ibid.* 76, 113 (1971); M. N. Toksoz, N. H. Sleep, A. T. Smith, *Geophys. J. R. Astron. Soc.* **35**, 285 (1973); D. L. Turcotte and G. Schubert, *J. Geophys. Res.* **78**, 5876 (1973); P. Bird, *Geophys. J. R. Astron. Soc.* **55**, 411 (1978); A. T. Hsui and M. N. Toksoz, *Tectonophysics* **60**, 43 (1979); K. P. Furlong *et al.*, *J. Geophys. Res.* **87**, 1786 (1982); S. Honda and S. Uyeda, in *Arc Volcanism: Physics and Tectonics*, D. Shimozuru and I. Yokoyama, Eds. (Terra Scientific, Tokyo, 1983), pp. 117–140; J. van der Beukel and R. Wortel, *Geol. Mijnbouw* **65**, 133 (1986); J. van der Beukel and R. Wortel, *Geophys. Res. Lett.* **14**, 1057 (1987). For a review, see S. M. Peacock, *Metamorphic Pressure-Temperature-Time Paths*, F. S. Spear and S. M. Peacock, Eds. (*Short Course in Geology, vol.* 7, American Geophysical Union, Washington, DC, 1989), pp. 57–102.
36. J. M. Delany and H. C. Helgeson, *Am. J. Sci.* **278**, 638 (1978).
37. R. N. Anderson, S. Uyeda, A. Miyashiro, *Geophys. J. R. Astron. Soc.* **44**, 333 (1976); R. N. Anderson *et al.*, *J. Geol.* **86**, 731 (1978); *ibid.* **88**, 445 (1980).
38. The subduction zone thermal structure and P-T-t paths presented in this paper are based on a two-dimensional numerical heat transfer model described in (*39, 40*); S. M. Peacock, *Eos* **69**, 1443 (1988).
39. S. M. Peacock, *J. Geophys. Res.* **92**, 12763 (1987).
40. ———, *Tectonics*, in press.
41. See, for example, D. P. McKenzie, *Geophys. J. R. Astron. Soc.* **18**, 1 (1969); D. J. Andrews and N. H. Sleep, *ibid.* **38**, 237 (1974); L. Bodri and B. Bodri, *Tectonophysics* **50**, 163 (1978).
42. Most estimates of shear stresses in subduction zones are on the order of 200 bars or less [J. N. Brune, *J. Geophys. Res.* **75**, 4997 (1970); N. H. Sleep, *Geophys. J. R. Astron. Soc.* **42**, 827 (1975); P. Bird, *ibid.* **73**, 2225 (1978)]. It is unlikely that higher shear stresses could be maintained in rocks undergoing dehydration reactions or in rocks at temperatures close to their melting point [H. C. Heard and W. W. Rubey, *Geol. Soc. Am. Bull.* 77, 741 (1966); D. A. Yuen, L. Fleitout, G. Schubert, C. Froidevaux, *Geophys. J. R. Astron. Soc.* **54**, 93 (1978)].
43. Based on numerical experiments for a subduction zone with velocity $v = 3$ cm year^{-1} (*38*). Prograde metamorphic reactions were modeled as consuming 50 kJ kg^{-1} on the basis of the heat consumed by the breakdown of tremolite at 30 kbar (*36*).
44. See, for example, W. G. Ernst, *Geology* **16**, 1081 (1988).
45. R. G. Coleman and M. A. Lanphere, *Geol. Soc. Am. Bull.* **82**, 2397 (1971); E. D. Ghent and R. G. Coleman, *ibid.* **84**, 2471 (1973); E. H. Brown and J. Y. Bradshaw, *Contrib. Mineral. Petrol.* **71**, 67 (1979); D. E. Moore, *J. Petrol.* **25**,

126 (1979); M. Cloos, *Tectonics* **4**, 421 (1985).
46. J. P. Platt, *Geol. Soc. Am. Bull.* **86**, 1337 (1975); S. S. Sorensen, *Geol. Soc. Am. Mem.* **164**, 59 (1986); ——— and M. D. Barton, *Geology* **15**, 115 (1987); S. S. Sorensen, *J. Metamorph. Geol.* **6**, 405 (1988).
47. G. E. Bebout and M. D. Barton, *Geology* **17**, 976 (1989).
48. S. M. Peacock and P. J. Norris, *J. Metamorph. Geol.* **7**, 191 (1989).
49. E. Knoebl and S. M. Peacock, *Geol. Soc. Am. Abstr. Prog.* **21**, A276 (1989).
50. Calculated using the thermodynamic data of R. G. Berman [*J. Petrol.* **29**, 445 (1988)] and the GEOCALC program of T. H. Brown, R. G. Berman, E. H. Perkins [*Comput. Geosci.* **14**, 279 (1988)].
51. See, for example, K. Yamamoto and S. Akimoto, *Am. J. Sci.* **277**, 288 (1977).
52. A. L. Boettcher and P. J. Wyllie, *J. Geol.* **76**, 314 (1968); W. Johannes and D. Puhan, *Contrib. Mineral. Petrol.* **31**, 28 (1971); W. D. Carlson and J. L. Rosenfeld, *J. Geol.* **89**, 615 (1981).
53. F. S. Spear, *Am. J. Sci.* **281**, 697 (1981); J. G. Liou, S. Maruyama, M. Cho, *Mineral. Mag.* **49**, 321 (1985).
54. See, for example, articles in B. W. Evans and E. H. Brown, Eds., *Geol. Soc. Am. Mem.* **164**, (1986).
55. C. B. Raleigh and M. S. Paterson, *J. Geophys. Res.* **70**, 3965 (1965).
56. C. B. Raleigh, *Geophys. J. R. Astron. Soc.* **14**, 113 (1967); C. Meade and R. Jeanloz, *Eos* **70**, 1321 (1989).
57. Fluid infiltration can drive devolatilization reactions. The P-T stability field of a hydrous mineral is greatest in the presence of a pure H_2O fluid. Diluting the fluid phase with a component such as CO_2 reduces the stability field of a hydrous mineral. Thus, infiltration of a CO_2-bearing fluid into a rock can drive dehydration reactions; conversely, infiltration of H_2O-rich fluids can drive decarbonation reactions.
58. S. M. Peacock, *Geology* **15**, 1057 (1987).
59. P. Fryer, E. L. Ambos, D. M. Hussong, *Geology* **13**, 774 (1985).
60. S. M. Peacock, *Contrib. Mineral. Petrol.* **95**, 55 (1987).
61. See, for example, Y. Tatsumi, *J. Geophys. Res.* **94**, 4697 (1989).
62. J. D. Morris and S. R. Hart, *Geochim. Cosmochim. Acta* **47**, 2015 (1983); R. K. O'Nions, *Phil. Trans. R. Soc. London* **A310**, 591 (1984); W. M. White and P. J. Patchett, *Earth Planet. Sci. Lett.* **67**, 167 (1984); G. Faure, *Principles of Isotope Geology* (Wiley, New York, ed. 2, 1986); R. W. Kay, *ibid.*, p. 535. Island arc volcanic rocks from the South Sandwich Islands and the Lesser Antilles are enriched in radiogenic ^{87}Sr relative to mantle Sr; these data suggest that altered oceanic crust is contributing to arc magmas [C. J. Hawkesworth, R. K. O'Nions, R. J. Pankhurst, P. J. Hamilton, N. M. Evensen, *Earth Planet. Sci. Lett.* **36**, 253 (1977); C. J. Hawkesworth, R. K. O'Nions, R. J. Arculus, *ibid.* **45**, 237 (1979); J. P. Davidson, *Geochim. Cosmochim. Acta* **51**, 2185 (1987)]. Volcanic rocks from the Banda island arc (Indonesia) have Nd-Sr systematics that strongly suggest contamination by subducted terrigenous sediment derived from old continental crust [D. J. Whitford, W. M. White, P. A. Jezek, *Geochim. Cosmochim. Acta* **45**, 989 (1981)].
63. Created in the upper atmosphere, ^{10}Be is transported to the Earth's surface by precipitation where it partitions strongly onto soil and sediment. ^{10}Be concentrations are $>10^3$ times as great in pelagic sediments as in mid-ocean ridge and oceanic island basalts. Significantly elevated ^{10}Be concentrations have been found in lavas from the Japan, Aleutian, and Central American arcs, but not in lavas from the Mariana and Halmahera arcs. The 1.5 million year half-life of ^{10}Be demands relatively rapid (<10 million years) recycling of sediments in subduction zones in order to account for the elevated ^{10}Be concentrations in arc lavas. F. Yiou and G. M. Raisbeck, *Phys. Rev. Lett.* **29**, 372 (1972); S. Tanaka and T. Inove, *Earth Planet. Sci. Lett.* **49**, 34 (1980); L. Brown *et al.*, *Nature* **299**, 718 (1982); F. Tera, L. Brown, J. Morris, I. S. Sacks, *Geochim. Cosmochim. Acta* **50**, 535 (1986); J. D. Morris, W. P. Leeman, F. Tera, *Nature* **344**, 31 (1990).
64. C. R. Stern and P. J. Wyllie, *Am. Mineral.* **63**, 641 (1978); T. Sekine, P. J. Wyllie, D. R. Baker, *ibid.* **66**, 938 (1981).
65. Dry solidus, hornblende-out curve is from T. H. Green, in *Andesites*, R. S. Thorpe, Ed. (Wiley, New York, 1982), pp. 465–487; wet solidus is from I. B. Lambert and P. J. Wyllie, *J. Geol.* **82**, 88 (1972).
66. See, for example, Y. Hariya and S. Terada, *Earth Planet. Sci. Lett.* **18**, 72 (1973); M. C. Gilbert, T. H. Rosalind, R. K. Popp, F. S. Spear, in *Amphiboles: Petrology and Experimental Phase Relations*, D. R. Veblen and P. H. Ribbe, Eds. (*Rev. Mineral.* **9B**, Mineralogical Society of America, Washington, DC, 1982), pp. 229–353.
67. Dry solidus, E. Takahashi and I. Kushiro, *Am. Mineral.* **68**, 859 (1983); wet solidus, B. O. Mysen and A. L. Boettcher, *J. Petrol.* **16**, 520 (1975); hornblende out, D. H. Green, *Earth Planet. Sci. Lett.* **19**, 37 (1973); phlogopite out: R. F. Wendlendt and D. H. Eggler, *Am. J. Sci.* **280**, 385 (1980).
68. MgO-SiO_2-H_2O phases are from (*51*); S. Kitahara, S. Takenouchi, G. C. Kennedy, *Am. J. Sci.* **264**, 223 (1966).
69. I thank G. E. Bebout, M. Cloos, W. G. Ernst, J. Holloway, and J. Tyburczy for helpful discussions regarding fluids in subduction zones. This work was supported by National Science Foundation grant EAR-8720343.

Mantle Oxidation State and Its Relationship to Tectonic Environment and Fluid Speciation

BERNARD J. WOOD, L. TARAS BRYNDZIA, KATHLEEN E. JOHNSON

The earth's mantle is degassed along mid-ocean ridges, while rehydration and possibly recarbonation occurs at subduction zones. These processes and the speciation of C-H-O fluids in the mantle are related to the oxidation state of mantle peridotite. Peridotite xenoliths from continental localities exhibit an oxygen fugacity (f_{O_2}) range from −1.5 to +1.5 log units relative to the FMQ (fayalite-magnetite-quartz) buffer. The lowest values are from zones of continental extension. Highly oxidized xenoliths (f_{O_2} greater than FMQ) come from regions of recent or active subduction (for example, Ichinomegata, Japan), are commonly amphibole-bearing, and show trace element and isotopic evidence of fluid-rock interaction. Peridotites from ocean ridges are reduced and have an average f_{O_2} of about −0.9 log units relative to FMQ, virtually coincident with values obtained from mid-ocean ridge basalt (MORB) glasses. These data are further evidence of the genetic link between MORB liquids and residual peridotite and indicate that the asthenosphere, although reducing, has CO_2 and H_2O as its major fluid species. Incorporation of oxidized material from subduction zones into the continental lithosphere produces xenoliths that have both asthenospheric and subduction signatures. Fluids in the lithosphere are also dominated by CO_2 and H_2O, and native C is generally unstable. Although the occurrence of native C (diamond) in deep-seated garnetiferous xenoliths and kimberlites does not require reducing conditions, calculations indicate that high Fe^{3+} contents are stabilized in the garnet structure and that f_{O_2} decreases with increasing depth.

THE MANTLE, REPRESENTING THAT VOLUME OF THE EARTH below the crust (10 to 40 km) and above the core (at 3200 km depth), may be presumed to have oxidation states ranging from equilibrium with Fe metal at the core-mantle boundary up to equilibrium with Fe^{3+}-rich silicate melts in the near-surface region. In this range, most major elements (for example, Si,